(1991 SCA Conference Paper Number 9128)

COMPUTERIZED NEUTRON TOMOGRAPHY FOR CORE ANALYSIS

R.C. Lanza, E.W. McFarland and G.W. Poulos
Department of Nuclear Engineering
Massachusetts Institute of Technology
Cambridge, MA 02139

ABSTRACT

The imaging of core samples using both x-ray computerized tomography (CT) and nuclear magnetic resonance (NMR) have shown the usefulness of imaging techniques as ways of measuring the porosity of saturated cores by producing images of the hydrogen content. In this paper, we describe a method for tomographic imaging using thermal neutrons which has the advantage of imaging directly the hydrogen content of samples with high sensitivity. We have made three dimensional images of a brine-saturated sample of San Andres dolomite using thermal neutrons from the MIT research reactor. The interaction of thermal neutrons varies greatly from element to element but the interaction probability is particularly large for hydrogen. As an example, the absorption length for SiO_2 is approximately 0.3 cm^{-1} while water is approximately 3.4 cm^{-1}. This is in marked contrast to x-ray CT where materials of high atomic number dominate the absorption. The mineral matrix is essentially transparent to the neutrons and thus neutron CT images provide a direct way to image the water or hydrocarbon content of cores and hence to obtain porosity information. The neutron absorption of typical steel core holders is also relatively small, and it is possible to image cores while they are inside steel core barrels.

BACKGROUND

X-ray tomography has been used in core analysis to determine density and elemental composition, and for fluid flow studies. The detailed spatial information available from CT imaging permits the determination of these properties even when samples are damaged or are highly inhomogeneous. (1) A refinement of the basic CT system is the use of dual-energy imaging. At high x-ray energies (above 100 keV), the dominant x-ray interaction on materials is Compton scattering which is essentially dependent only on the bulk density of the material and does not provide a method for separation of materials by atomic number. Below 100 keV, the interaction is dominated by photoelectric absorption which is strongly dependent on the atomic number of the material. By comparing images taken at two energies, it is possible to separate out elements and thus to determine to some extent the composition of the rock. Unfortunately, except at the lowest energies, the interaction of x-rays with hydrogen bearing materials is dominated by Compton scattering and as a result, the imaging of hydrocarbons in rocks is therefore less sensitive. Modern medical CT systems are designed to image essentially uniform, low absorption objects (soft tissue) with inclusions of small amounts of high absorption material (bone). For core imaging, the inverse situation exists with a small amount of low-absorption hydrocarbon distributed within the high absorption rock matrix. Software reconstruction algorithms have been modified so as to enhance the imaging of hydrocarbons and water in this case. In addition, the significant absorption of low energy x-rays by steel core barrels reduces further the ability to image hydrocarbons directly.

Nuclear Magnetic Resonance (NMR) imaging provides a means for measuring directly the distribution of hydrogen containing fluids in samples and can be used to distinguish between oil and water due to the differences in relaxation times and chemical shift (2). Fluid porosity, oil saturation and pore size can be measured using NMR. As with CT, the imaging process provides the means to distinguish the spatial variations of these properties but the core samples must be in non-metallic holders and imaging is limited to those samples which are not excessively conductive or magnetic. (2)

Tomographic imaging using thermal neutrons provides a unique method for measuring properties of cores (3). The basic technique is similar to x-ray CT but neutron CT is capable of directly visualizing hydrogen distributions while the mineral structure of the rock is essentially transparent. It is thus possible to measure the porosity of materials by direct measurement of the spatial distributions of hydrocarbons or water. This is in marked contrast to the situation with x-rays where hydrocarbons are relatively transparent. Thus, neutron imaging provides complementary information to that obtained from x-rays. To see this, the interactions of x-rays and neutrons are compared in Figure 1 which shows the mass absorption coefficient of x-rays and of thermal neutrons as a function of atomic number. Several features are illustrated here. Whereas x-rays are strongly absorbed by heavy elements and poorly absorbed by light elements, dramatically different attenuation characteristics are observed for neutrons. Low-energy neutrons can interact strongly with light elements and minimally with heavy elements. Additionally, due to details of nuclear structure, neutrons can have interaction properties different by several orders of magnitude between nuclei, with small differences in atomic number. The absorption for hydrogen is orders of magnitude larger than for materials such as aluminium, silicon, and oxygen. (Note that the vertical scale is logarithmic in mass absorption and that the absorption will be exponential in the absorption coefficient.)

Planar radiographic techniques are limited, due to the nature of the image production. Density variations in the radiograph represent the integrated interaction cross-section over the entire path of radiation through the object Details of internal structure are easily hidden in this effective averaging. Tomography using the method of image reconstruction from projections allows two- and three-dimensional detail to be retained and the object to be visualized in cross-section, retaining the spatial distribution of radiation attenuation and thus the details of the object's internal structure. Attenuation differences as little as 0.02% have been measured with computer-aided x-ray tomography [4]. Neutron-computed tomography (NCT) imaging is less restricted because differences in neutron cross-section will often vary by orders of magnitude, and it thus offers the potential of increases in sensitivity for imaging hydrocarbons in cores while retaining the spatial resolution of x-ray CT.

The use of thermal neutrons has considerable advantages for the analysis of cores particularly when hydrocarbons or water are to be imaged. The primary advantage comes in contrast resolution and as a result, sensitivity to porosity. If we consider a simple example, assuming a fully saturated sample, then the effective absorption length will be given by:

$$\mu_{eff} = p\mu_{oil} + (1-p)\mu_{mat}$$

where μ_{oil} and μ_{mat} are the absorption length for oil and the matrix and p is the porosity defined as the volume fraction occupied by the pores,

$$\frac{d\mu_{eff}}{dp} = \mu_{oil} - \mu_{mat}$$

The error in porosity is given by:

$$dp = \left(\frac{d\mu}{\mu}\right)\left(\frac{\mu_{eff}}{\mu_{oil} - \mu_{mat}}\right)$$

From this, we see the intuitive requirement that the most sensitive situation is when the absorption of the material in the pores is much larger than that of the matrix material. Table 1 compares the absorption coefficients for x-rays at 100 keV and for thermal neutrons.

TABLE 1
Absorption coefficients (cm^{-1})

Material	SiO_2	oil	H_2O	Al	Fe
100 keV x-rays	0.45	0.14	0.17	0.4	1.5
Neutrons	0.3	3.4	3.4	0.1	1.1

The fundamental limitation on image quality from neutron tomography or indeed any transmission imaging method is the quantum nature of the image formation process. Practical considerations, including time constraints, will limit the spatial resolution of neutron tomography at present: specifically, the neutron source, detector spatial resolution, and scatter discrimination.

In principle, spatial resolution is limited by the resolution of the scintillator screen. Beam divergence causing geometric blurring will, however, limit resolution in many practical parallel beam imaging configurations. The optical flare of the lens and mirror system would also contribute to degradation of resolution below 20-30 microns.

Contrast resolution, as is the case for x-ray CT, will be determined by the radiation counting statistics. Our goal is to detect a difference $d\mu$ in the macroscopic cross-section $\mu(x,y,z)$ in a volume element ΔV. Considering a purely absorbing medium, if N_j particles enter V_j, and N_{j+1} exit without interacting, the variation in the number exiting due to the variation $d\mu$ will be:

$$\Delta N = d\mu \, \Delta x \, N_j$$

In order to detect the fractional difference, $\frac{d\mu}{\mu}$,

our detector statistical error, $\sqrt{N}$, must be, at worst, ΔN, therefore:

$$\sqrt{N} \leq \left[\frac{d\mu}{\mu}\right](\Delta x \mu)N_j$$

where N_j is the number of counts in the detector. If we take an ideal, purely absorbing medium as the worst case situation and assume an ideal reconstruction algorithm, then the minimum detectable $\left[\frac{d\mu}{\mu}\right]$ can be

calculated in a cubic voxel $\Delta x = \Delta y = \Delta z = \Delta r$. For an incident intensity $N_0 = F(\Delta r)^2 t$, an average macroscopic absorption cross-section, μ, and an object of size D, the detectable difference in is:

$$\left[\frac{d\mu}{\mu}\right] = \sqrt{\frac{e^{\mu D}}{(\Delta r)^4 \mu^2 F t}}$$

where F is the flux in neutrons/cm^2/sec. Effectively, neutron imaging sees only the hydrocarbon or water in a specimen and measures it directly. Although water and oil have the same absorption for neutrons, it will be possible to measure water separately by doping it with a neutron absorber such as boron and hence it should be possible to separate the two. Table 2 shows values for these parameters for a voxel of 1 mm^3 and for a total fluence of 10^9 neutrons. Core diameters of from 1" to 3" diameter are shown. The absorption of a 1/8" steel core barrel and a 1/8" mud layer are also included.

METHODS

The basic theory underlying tomography is the same for both neutrons and x-rays (1,3). A parallel or fan beam of radiation is incident on the object to be imaged. The attenuation of the incident beam is measured to form a projection of the object onto a detector array. A series of projections taken at different angles is then reconstructed to form a two-dimensional image of the cross-section of the object. Successive "slices" are taken by moving the object along its rotation axis to form a complete three-dimensional reconstruction of the object. In the usual x-ray based CT scanner, a single fan beam of radiation is detected by a linear detector array to form the complete projection for a given angle. For the neutron tomography system, we employed a two-dimensional detector array and as a result were able to take many slices of data simultaneously, thereby speeding up the data collection process. Data acquisition consists of taking a two dimensional image, rotating the sample, and taking the next in a series of images.

The experimental arrangement of the system is shown schematically in Fig. 2. A rectangular-shaped beam (5 cm x 5 cm) of approximately parallel neutrons $(\Delta\theta = \pm 1.2^\circ)$ with a flux of 2.4 x 10^8 n/cm^2/sec is extracted from the reactor source. The sample to be imaged is placed on a rotating sample holder in line with the beam. Neutrons passing through the sample are absorbed in the scintillator screen; photons generated in the screen pass through a lens and enter the charge-coupled device (CCD) detector, which is a rectangular array of n x m pixels. The photo-electrons generated at each CCD pixel comprise the electrical signal and are proportional to the number of neutrons detected in the screen.

The detector developed for this study is a two-dimensional integrating detector, based on an electro-optical configuration (3). The detector is shown schematically in Fig. 3. For the detection of neutrons, a ^{6}LiF-ZnS (Nuclear Enterprises NE426) scintillator was used, which is imaged onto a cooled charge-coupled device (CCD) imager by means of a front-surfaced mirror and lens. The NE426 screen has been optimized for use with film and emits a blue-green light, which is not optimal for the cooled CCD response. The wavelength for peak efficiency of the CCD differs from film and typically is most sensitive to red photons. Y_2O_3:Eu and $(Zn,Mg)_3(PO_4)_2$:Mn_4 screen mixtures have ideal phosphor wavelengths; however, we chose the NE426 screen because it was commercially available. The NE426 with LiF screen has a detection efficiency of 0.15 (15%) for thermal neutrons incident perpendicular to the screen and a light output of 1.7×10^5 photons per neutron (3).

Photons generated in the scintillator phosphor are reflected by the front-surfaced mirror and pass through a lens prior to entering the CCD. This geometry allows the CCD to be shielded from the incident neutron beam and thereby prevents damage to the detector. Also, noise from neutron activation, which has been reported by others, is eliminated. The assembly was enclosed in a light-tight aluminum box. The CCD was used in an integrating mode and is read out into a data acquisition and display computer. The choice of CCD type depends on the required spatial resolution of the system. The NE426 scintillator screen has a resolution of 0.1 mm when used in its intended configuration with conventional film, and this can be preserved (and perhaps improved) through the lens-CCD system. For this study, we used two different CCD cameras, a Microluminetics Cryocam-80 (Microluminetics, Inc., Los Angeles, California) with a 572 x 480 pixel array with 15 micron pixels and a Hamamatsu camera with a 1000 x 1018 pixel CCD with 13 micron pixels (Hamamatsu Photonics, Bridgewater, New Jersey). More complete details of the system design and of its performance are to be found in (3).

RESULTS

Using this system, tomographic images were taken of a 2.54 cm. diameter core of San Andres dolomite saturated with distilled H_2O. Images were taken at 45 different angles to reconstruct the full three dimensional image. The imaging system has a resolution of 0.065 mm per pixel, however , the resolution of the scintillator screen and optics was approximately 0.2 mm. Each image took approximately 4 seconds for a total imaging time of three minutes. Although data were taken in a 1000 x 1000 pixel array, only data from a 32 pixel high slice were used for reconstruction purposes. Figure 4 shows a projection neutron radiograph of the core while Figure 5 shows a stacked three-dimensional reconstruction showing structure in the axial direction. Increased neutron attenuation by porous regions of the sample where water accumulation occurs is darker than the surrounding areas. In Figure 6 several slices obtained by 120 kVp x-ray CT (right) are shown with the approximate corresponding neutron CT slice (left) (5). Clearly more internal details are visualized in the neutron image.

DISCUSSION

A major limitation of this technique at the present time is the availability of large fluence neutron sources which are not reactor based. For example, using a conventional D-T neutron generator, 14 MeV neutron outputs of 10^9 n/s are possible. However, after moderation and collimation, the fluence of collimated, thermalized neutrons will be of the order of 10^5 n/cm^2/s. As a result, the total measurement time will be approximately 10^4 s or three hours to achieve the results shown in Table 2. Although this will still be adequate for research purposes, a more robust source will clearly improve the practical applicability of this technique.

Accelerator based systems appear to be the most likely approach which meets the need for portability, neutron flux, and safety. A larger variation of the D-T technique has been developed which produces 10^{11} n/s. Another class of accelerator uses a reaction such as $Li^7(p,n)$ to produce neutrons. This reaction requires protons of 2 MeV which can be obtained either from a DC accelerator or an RF quadrupole accelerator (RFQ) and can produce more than 10^{12} n/s.

The most interesting new source to date appears to be the pulsed plasma focus source. These sources are considerably smaller than conventional accelerators and potentially could be lower in cost. They have demonstrated 14 MeV neutron outputs of 4×10^{11} neutrons/pulse which would result in a thermal neutron fluence of perhaps 4×10^7 n/cm^2/pulse. Each view would then be taken in a single pulse with a total of 180 pulses or less depending on the reconstruction matrix size required. The total elapsed time would be of the order of 5 minutes or less. The development of such a source would provide a highly portable source of neutrons for tomography and in addition, the pulsed nature of the neutrons from this source may permit additional enhancements. The major problem with this source concerns its long term reliability and reproducibility when compared to the more conventional sources. Although current designs have produced large fluxes of neutrons, they have generally been used in experimental laboratory situations where only a few thousand pulses are required and thus will require additional development. Source development is the major technical challenge remaining for practical neutron imaging.

ACKNOWLEDGEMENTS

We wish to acknowledge and thank the Microluminetics Corp. and Hamamatsu Photonics for the use of cooled CCD cameras as well as the MIT Sloan Fund and the companies participating in the MIT International Program for Enhanced Nuclear Power Plant Safety for partially funding this research. The help of the MIT Reactor staff is also acknowledged, and we are also grateful to Ms. Jennifer Uhle for her technical assistance. We especially thank Harold Vinegar of Shell Development Co. for encouraging our work in this area and for providing samples and advice throughout this project.

REFERENCES

1. S.L. Wellington and H.J. Vinegar, "X-ray Computed Tomography", J. Pet. Tech., v39,pp 885 -898, 1987

2. W. A. Edelstein, H. J. Vinegar, P.N. Tutunjian, P. B. Roemer, and O. M. Mueller, "NMR imaging for core analysis". Soc. Pet. Eng. 18272, pp 101 - 112 (1988)

3. E. W. McFarland, R. C. Lanza, and G.W. Poulos, "Multi-dimensional Neutron-computed Tomography Using Cooled Charge-coupled Devices", IEEE Trans. on Nuc. Sci, v. 38, pp 612-622 (1991)

4. C. E. Cann and H. K. Genant, "Precise measurement of vertebral mineral content using computed tomography," J. Comput. Assist. Tomogr., 4, p. 493, 1980.

5. provided by H. Vinegar, Shell Development Co.

TABLE 2

wall thickness (")		0.125						
wall transmission		0.474						
mud layer (")		0.125						
mud transmission (thickness = 2 x wall)		0.113						
voxel (mm)	1.00							
fluence (n/cm2)	10^9							
	core OD"							
porosity		0%	5%	10%	15%	20%	25%	30%
μ effective		0.26	0.42	0.58	0.74	0.90	1.06	1.22
	1.00							
transmission		2.75E-02	1.84E-02	1.23E-02	8.19E-03	5.47E-03	3.65E-03	2.44E-03
$d\mu/\mu$ (%)		7.30%	5.55%	4.93%	4.73%	4.77%	4.96%	5.27%
dp		0.60%	0.73%	0.90%	1.10%	1.35%	1.65%	2.01%
	1.50							
transmission		1.97E-02	1.08E-02	5.87E-03	3.21E-03	1.75E-03	9.55E-04	5.21E-04
$d\mu/\mu$ (%)		8.61%	7.25%	7.12%	7.57%	8.43%	9.69%	11.40%
dp		0.71%	0.96%	1.30%	1.76%	2.38%	3.22%	4.36%
	2.00							
transmission		1.41E-02	6.31E-03	2.81E-03	1.26E-03	5.60E-04	2.50E-04	1.11E-04
$d\mu/\mu$ (%)		10.17%	9.47%	10.29%	12.09%	14.90%	18.95%	24.66%
dp		0.84%	1.25%	1.88%	2.81%	4.20%	6.30%	9.43%
	2.50							
transmission		1.01E-02	3.70E-03	1.35E-03	4.91E-04	1.79E-04	6.53E-05	2.38E-05
$d\mu/\mu$ (%)		12.01%	12.37%	14.87%	19.32%	26.33%	37.05%	53.34%
dp		0.99%	1.64%	2.71%	4.49%	7.43%	12.31%	20.39%
	3.00							
transmission		7.28E-03	2.17E-03	6.46E-04	1.92E-04	5.73E-05	1.71E-05	5.09E-06
$d\mu/\mu$ (%)		14.17%	16.15%	21.48%	30.88%	46.55%	72.46%	115.39%
dp		1.17%	2.14%	3.91%	7.17%	13.14%	24.07%	44.11%

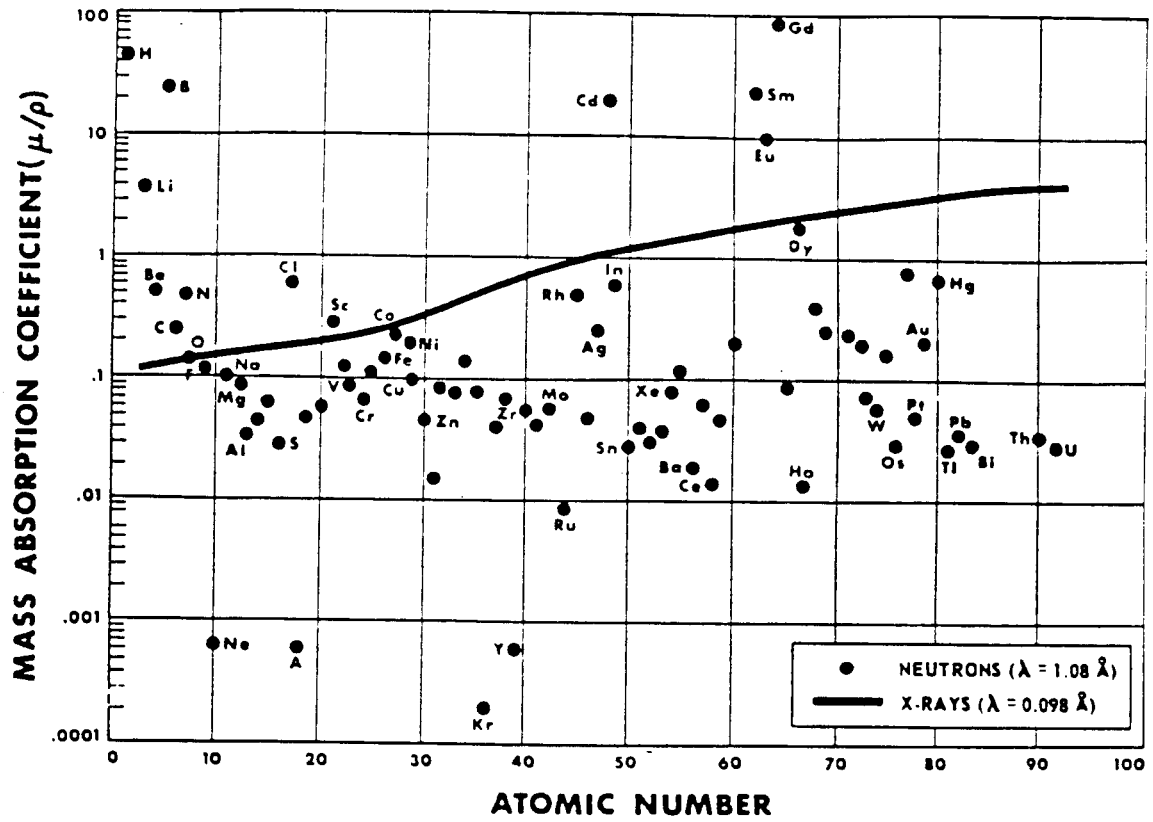

A comparison of mass absorption coefficients for the elements for both X-rays and thermal neutrons. More extensive comparison data are given in Table 1. After THEWLIS (1956, 1958). (Courtesy Argonne National Laboratory.)

Figure 1. Comparison of Neutron and X-ray absorption.

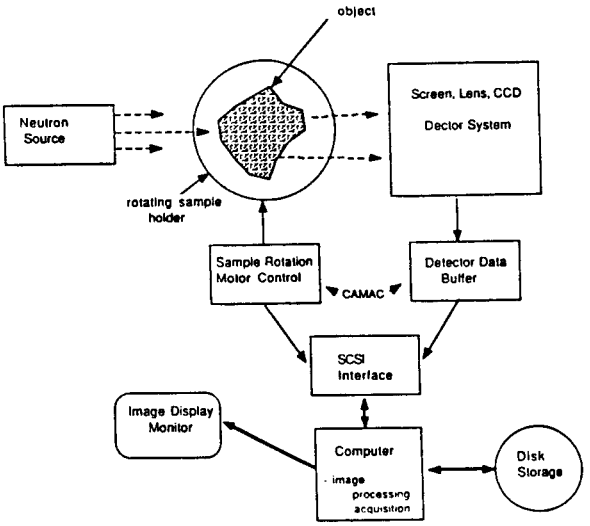

Figure 2. Experimental Arrangement

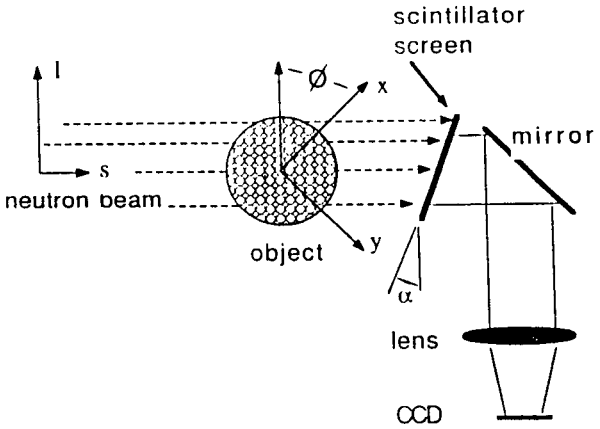

Figure 3. Neutron imaging detector

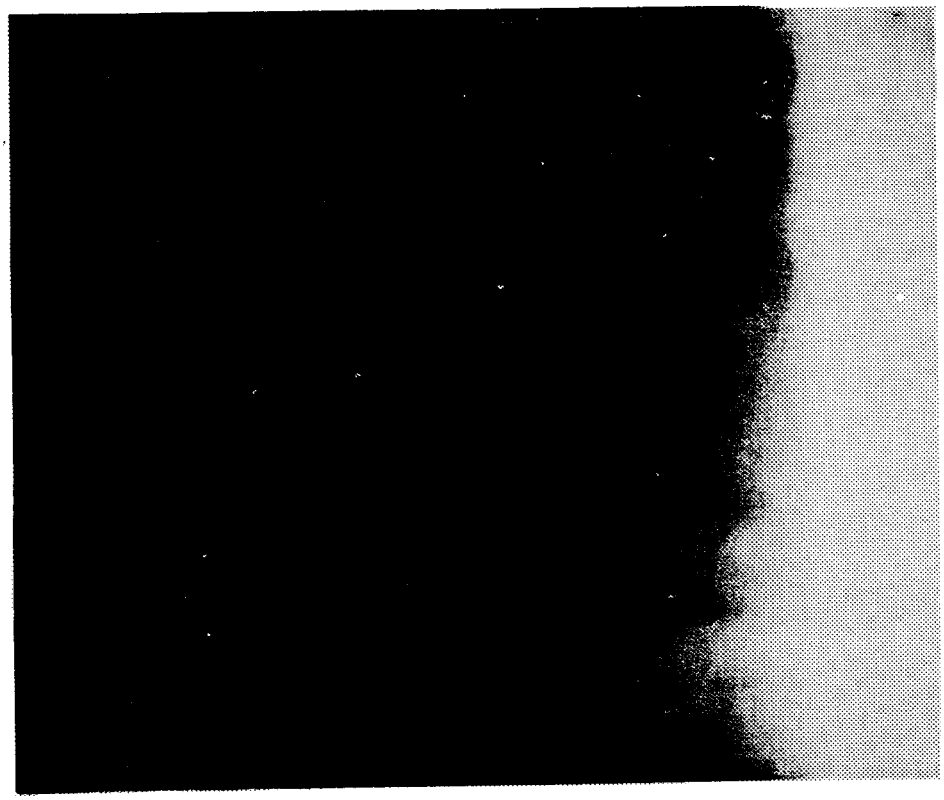

Figure 4. Projection neutron radiograph of core.

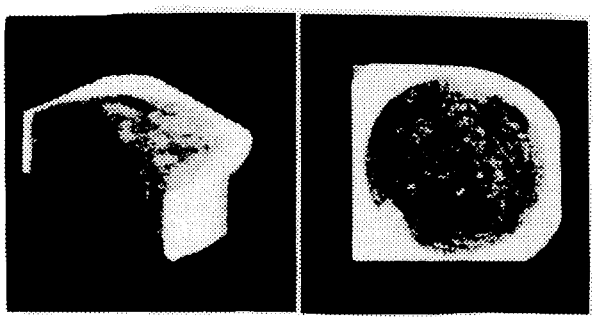

Figure 5. Stacked three-dimensional neutron image of core.

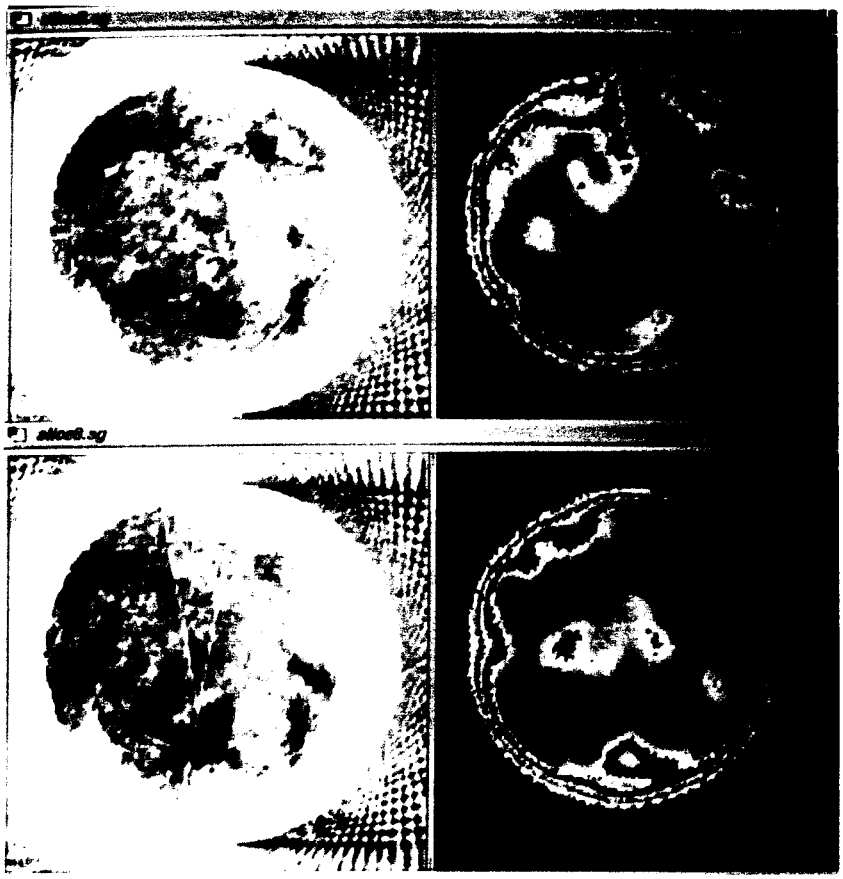

Figure 6. Cross-sectional slices using neutrons (left) and100 keV x-rays (right).